

## Crosstalk between the H3K36me3 and H4K16ac histone epigenetic marks in DNA double-strand break repair

Lin Li and Yinsheng Wang\*

Department of Chemistry, University of California, Riverside, California 92521-0403.

Running Title: H3K36me3 and H4K16ac Crosstalk in DSB Repair

\*Corresponding Author: Yinsheng Wang, Tel.: (951) 827-2700; Fax: (951) 827-4713;

E-mail: Yinsheng.Wang@ucr.edu

**Key Words:** DNA repair, epigenetics, post-translational modification, histone methylation, histone acetylation.

### Abstract

Post-translational modifications of histone proteins regulate numerous cellular processes. Among these modifications, trimethylation of lysine 36 in histone H3 (H3K36me3) and acetylation of lysine 16 in histone H4 (H4K16ac) have important roles in transcriptional regulation and DNA damage response signaling. However, whether these two epigenetic histone marks are mechanistically linked remains unclear. Here, we discovered a new pathway through which H3K36me3 stimulates H4K16ac upon DNA double-strand break (DSB) induction in human cells. In particular, we examined, using Western blot analysis, the levels of H3K36me3 and H4K16ac in cells after exposure to various DSB-inducing agents, including neocarzinostatin,  $\gamma$  rays and etoposide, and found that H3K36me3 and H4K16ac were both elevated in cells upon these treatments. We also observed that the DSB-induced H4K16 acetylation was abolished in cells upon depletion of the histone methyltransferase gene *SET-domain containing 2* (*SETD2*) and the ensuing loss of H3K36me3. Furthermore, the H3K36me3-mediated increase in H4K16ac necessitated lens

epithelium-derived growth factor p75 splicing variant (LEDGF), which is a reader protein of H3K36me3, and the KAT5 (TIP60) histone acetyltransferase. Mechanistically, the chromatin-bound LEDGF, through its interaction with KAT5, promoted chromatin localization of KAT5, thereby stimulating H4K16 acetylation. Together, we unveiled a crosstalk between two important histone epigenetic marks and defined the function of this crosstalk in DNA DSB repair.

### Introduction

In eukaryotes, the package of genomic DNA into chromatin creates a physical barrier limiting the access of DNA by protein machineries involved in various activities of DNA metabolism including DNA repair (1,2). Thus, repair of DNA lesions in chromatin necessitates chromatin remodeling, histone exchange and/or post-translational modifications of histones (3).

Among the plethora of post-translational modifications of histone proteins, methylation of lysine 36 in histone H3 (H3K36) is a key and widespread modification on chromatin, and it has been implicated in RNA splicing as well as DNA

replication, transcription, methylation and repair (4-6). In mammalian cells, mono-, di- and trimethylation of H3K36 (H3K36me, H3K36me2 and H3K36me3) are catalyzed by distinct methyltransferases; nuclear SET domain (NSD)-containing methyltransferases, including NSD1, NSD2 and NSD3, induce H3K36me and H3K36me2, whereas SET domain-containing 2 (SETD2) is the major enzyme for catalyzing H3K36me3 (5). Previous studies showed that methylation of H3K36 plays important roles in DNA double strand break (DSB) repair (7-9) and mismatch repair (6). In mammalian cells, SETMAR (Metnase)-mediated H3K36me2 was found to be DNA damage-inducible and this methylation mark enables the recruitment and stabilization of NBS1 and Ku70 near DNA DSB sites, thereby promoting DSB repair via the non-homologous end-joining (NHEJ) pathway (10). In addition, the SETD2-catalyzed H3K36me3 enables the recruitment of CtIP to sites of DNA DSBs and promotes resection at DSB ends (7). Reducing H3K36me3 level through knockdown of *SETD2* or overexpression of an H3K36me2/3 demethylase gene, *KDM4A/JMJD2A*, in cells led to defective repair of DNA DSBs via the homologous recombination (HR) pathway (7,8). Moreover, H3K36me3 is required for the recruitment of the mismatch recognition protein hMutS $\alpha$  onto chromatin through interaction with the Pro-Trp-Trp-Pro (PWWP) domain of hMSH6, thereby enabling mismatch repair (6).

The H3K36me3-binding proteins LEDGF and MRG15 also promote DNA DSB repair (7,11-13). LEDGF specifically recognizes H3K36me3 via its PWWP domain, which stimulates the CtIP-mediated DNA end resection during HR-mediated repair of DNA DSBs (7,13). MRG15 is a conserved chromo domain protein, which binds specifically to H3K36me3 (14); after DNA damage, MRG15 interacts with PALB2 and activates the HR

pathway (11).

Acetylation of lysine 16 in histone H4 (H4K16ac) is another important histone modification that functions in DNA damage repair (15,16). hMOF and KAT5 are the two major acetyltransferases catalyzing the formation of H4K16ac (17-19). Incorporation of synthetic H4K16ac into nucleosomes prevents their compaction into 30 nm chromatin fibers *in vitro* (20). Additionally, H4K16ac level is up-regulated upon exposure to ionizing radiation (17), and this acetylation is thought to modulate DNA DSB repair pathway choice by favoring HR via promoting the chromatin localization of BRCA1 while restricting the binding of 53BP1 to chromatin (21,22).

Despite the importance of H3K36me3 and H4K16ac in DNA repair in mammalian cells, it remains elusive whether there exists a mechanistic link between these two histone epigenetic marks. In this context, Arabidopsis MRG domain proteins are known to bridge H3K36me3 and histone H4 acetylation for regulating flowering time (23). Therefore, we decided to assess the potential link between these two important histone epigenetic marks in mammalian cells. In the present study, we generated, by employing CRISPR/Cas9-based genome editing method, isogenic HEK293T cells depleted of *SETD2*, *LEDGF*, *MRG15* or *KAT5* gene, and analyzed the temporal responses of H3K36me3 and H4K16ac in these cells following exposure to neocarzinostatin (NCS), a DNA DSB-inducing agent. We found that DNA DSB induction stimulated a transient increase in H3K36me3, which enhanced the binding of LEDGF to chromatin, thereby promoting the chromatin localization of KAT5 and the acetylation of H4K16. Thus, our results uncovered a novel crosstalk between H3K36me3 and H4K16ac in the context of DNA DSB repair.

## Results

### **DNA DSB formation stimulated transient increases in H3K36me3 and H4K16ac, and the elevation in H4K16ac required SETD2.**

To examine whether there is a crosstalk between H3K36me3 and H4K16ac, we generated H3K36me3-deficient cells by knocking out the major H3K36 tri-methyltransferase SETD2 using the CRISPR/Cas9 genome-editing method (Fig. S1A) and examined the levels of these two histone epigenetic marks by Western blot analysis (Fig. 1). As expected, H3K36me3 was almost entirely abolished in *SETD2*<sup>-/-</sup> cells (Fig. 1), which is accompanied with a significant drop (by approximately 30%) in the basal level of H4K16ac (Fig. 1A-B), supporting that H3K36me3 promotes H4K16ac.

Because both H3K36me3 and H4K16ac function in DNA DSB repair, we next examined the temporal responses of these two histone epigenetic marks in HEK293T cells following exposure to NCS, a radiomimetic agent capable of inducing DNA DSBs in cells. We found that NCS exposure led to transient increases in the levels of H3K36me3 and H4K16ac in HEK293T cells, which peak at ~30 and 60 min, respectively, and return to nearly normal levels at approximately 4 hrs (Fig. 1C-F and Fig. S2). In addition, the time-dependent alteration in the level of H3K36me3 following NCS treatment mirrors that of  $\gamma$ -H2AX (Fig. 1D-E), which reflects the level of DNA DSBs (24). Similar transient increases in  $\gamma$ -H2AX, H3K36me3 and H4K16ac were also observed in HEK293T cells upon exposure to other DNA DSB-inducing agents, including  $\gamma$  rays and etoposide (Fig. S3). Furthermore, exposure of HeLa and U2OS cells to NCS also stimulated the elevation in H3K36me3 and H4K16ac (Fig. S4). We next asked whether this NCS-stimulated increase in H4K16ac requires SETD2-mediated H3K36me3. Indeed our results showed that genetic depletion of SETD2 in

HEK293T cells abolished the NCS-induced elevation in H4K16ac, though the NCS-triggered transient increase in  $\gamma$ -H2AX was not affected by the loss of SETD2 (Fig. 1C-F and Fig. S2). This result underscored that H3K36me3 is indispensable for the DNA damage-induced H4K16ac.

### **KAT5 is recruited to chromatin and induces H4K16ac upon DNA DSB induction, which are abolished in cells deficient in SETD2.**

Having demonstrated the dependence of H4K16 acetylation on H3K36me3 after DNA DSB induction, we next explored the histone acetyltransferases involved in this process by assessing the chromatin localizations of the two known H4K16 acetyltransferases, hMOF and KAT5, following NCS exposure (Fig. 1G-H). Our results revealed that NCS treatment did not elicit the chromatin localization of hMOF in HEK293T cells or the isogenic cells depleted of SETD2 (Fig. 1G). By contrast, the chromatin-bound KAT5 was substantially increased, by 1.6-1.9 fold, in HEK293T cells after NCS exposure, and this DNA damage-triggered chromatin localization of KAT5 was abrogated in HEK293T cells depleted of SETD2, though the expression level of KAT5 was not altered upon SETD2 depletion (Fig. 1H and Fig. S6). Hence, these results support that the DNA damage-stimulated recruitment of KAT5 to chromatin necessitates SETD2-mediated trimethylation of H3K36.

To further substantiate the above finding, we knocked out the *KAT5* gene in HEK293T cells (Fig. S1A) and assessed its effect on the temporal responses of H3K36me3 and H4K16ac after NCS exposure. Our results showed that, despite with the increase in H3K36me3, the level of H4K16ac in *KAT5*<sup>-/-</sup> cells did not change after NCS treatment, underscoring the crucial role of KAT5 in NCS-triggered H4K16ac (Fig. 2A-C and Fig. S5).

### **LEDGF functions in DNA damage-stimulated**

### increase in H4K16ac.

We next explored the reader proteins of H3K36me3 that transduce the signal from H3K36me3 to H4K16ac. In this respect, mortality factor 4-like protein 1 (MRG15) and lens epithelium-derived growth factor p75 splicing variant (LEDGF) were previously shown to bind to H3K36me3 through their chromo and PWWP domains, respectively (13,14), and both proteins function in DNA DSB repair (12,13). Hence, we also depleted *MRG15* and *LEDGF* genes using CRISPR/Cas9 (Fig. S1), and examined the impact of their depletion on the NCS-stimulated increase in H4K16ac. It turned out that genetic ablation of LEDGF, but not MRG15, abolished the NCS-induced elevation in H4K16ac (Fig. 2A-C Fig. S5 and Fig. S7). Similar to what we observed for *KAT5*<sup>-/-</sup> cells, the NCS-triggered elevation in H3K36me3 was still observed in *LEDGF*<sup>-/-</sup> cells (Fig. 2A-C and Fig. S5). In this vein, it is worth noting that the basal levels of H4K16ac were not changed upon depletion of *LEDGF* or *KAT5* gene (Fig. S7C). Therefore, our results support the crucial role of LEDGF in facilitating the DNA damage-induced H4K16ac.

### LEDGF interacts with H3K36me3 and KAT5 in cells, and promotes the DNA damage-induced recruitment of KAT5 to chromatin.

LEDGF possesses a conserved PWWP domain, which is characterized by its strong binding affinity toward methylated lysine in histone proteins (7,13,25). Thus, we examined the interaction between LEDGF and H3K36me3 by immunoprecipitation, where we employed Flag-tagged LEDGF and its variant form with two aromatic amino acid residues in the binding pocket of the PWWP domain being mutated to alanines to pull down H3K36me3 and histone H3. Our results showed that, although wild-type LEDGF could pull down histone H3 and H3K36me3, the PWWP domain mutant displayed markedly reduced

binding affinities toward H3K36me3 and histone H3 (Fig. 3A and results from another biological replicate are shown in Fig. S8A). We further assessed the chromatin localization of LEDGF in *SETD2*<sup>-/-</sup> cells. In HEK293T cells, substantial recruitment of LEDGF to chromatin could be observed after NCS treatment; genetic depletion of SETD2, however, led to a pronounced drop in the amount of LEDGF in the chromatin fraction (Fig. 3B and Fig. S8B-C). This result indicates a pivotal role of H3K36me3 in tethering LEDGF to chromatin.

We also assessed the role of LEDGF in KAT5's recruitment to chromatin (Fig. 3C-D). We found that the depletion of LEDGF, while not affecting the expression level of KAT5 protein (Fig. S6C), nearly abolished the DNA damage-stimulated localization of KAT5 to chromatin, which is similar to the observations made for *SETD2*<sup>-/-</sup> cells (Fig. 3D and Fig. S8D-E). The chromatin localization of hMOF, however, was not perturbed by the absence of LEDGF, which is independent of whether the cells are exposed with NCS (Fig. 3C).

We also investigated the interaction between LEDGF and KAT5 in cells. Plasmids for expressing HA-tagged KAT5 and Flag-tagged LEDGF were co-transfected into HEK293T cells, and reciprocal pulldown experiments revealed the interaction between the two ectopically expressed proteins (Fig. 3E-F and Fig. S8F-G). Similar immunoprecipitation experiments using lysates from cells transfected with HA-tagged KAT5 alone showed the interaction between the ectopically expressed KAT5 and endogenous LEDGF (Fig. 3G-H and Fig. S8H-I). It is worth noting that, we did not conduct pull-down experiments for monitoring the interaction between endogenous KAT5 and LEDGF owing to the lack of suitable antibody for endogenous KAT5. We, however, were not able to detect the interaction between recombinant LEDGF and KAT5 purified from

*Escherichia coli*, suggesting that the interaction between the two proteins may be indirect (i.e. involving other proteins in human cells) or modulated by post-translational modifications of LEDGF and/or KAT5. Cumulatively, our results support the notion that DNA DSB induction leads to increased H3K36me3, which stimulates the recruitment of LEDGF to chromatin through interaction via its PWWP domain and promotes the chromatin localization of KAT5.

**SETD2 and LEDGF play important roles in stimulating H3K36me3 and H4K16ac at a site-specifically generated DNA DSB site.**

Having demonstrated the responses in global levels of H3K36me3 and H4K16ac following DNA damage induction by NCS, we next examined the levels of H3K36me3 and H4K16ac in DNA regions surrounding an I-SceI-generated DNA DSB site using chromatin immunoprecipitation (ChIP) followed by real-time quantitative PCR analysis. Real-time PCR targets were located at approximately 500 and 2500 bp from the I-SceI-induced DNA DSB site in U2OS-DRGFP cells (Fig. 4A) (26). It turned out that the levels of H3K36me3 and H4K16ac at the proximal site (i.e. 500 bp from the DNA DSB locus) were pronouncedly elevated, whereas no substantial increases were found at the distal site (i.e. 2500 bp away from the DNA DSB site, Fig. 4B-C). After knockdown of *SETD2* or *LEDGF* by siRNA, the fold changes in H4K16ac enrichment at DNA DSB site were markedly diminished, again supporting that H3K36me3 and its reader protein LEDGF assume crucial roles in the DNA DSB-induced H4K16ac (Fig. 4B-C).

**Discussion**

Both H3K36me3 and H4K16ac were previously shown to be important in HR-mediated repair of DNA DSBs, where H3K36me3 stimulates the binding of CtIP to chromatin through LEDGF

(7-9) and H4K16ac promotes chromatin localization of BRCA1 by limiting the binding of 53BP1 to H4K20me2-marked chromatin (22). In the present study, we demonstrated, for the first time, that H3K36me3 can be stimulated by DNA DSB-inducing agents and that these two DNA damage signaling pathways are mechanistically coupled.

**H3K36me3 could be stimulated by DNA DSB-inducing agents.**

We provided multiple lines of evidence to support that H3K36me3 could be increased upon DNA DSB formation. In particular, we found that the global level of H3K36me3 increased gradually in HEK293T, HeLa and U2OS cells after NCS treatment, which peaks at ~30 min and returns to almost normal level at approximately 4 hrs (Fig. 1C&E, Fig. S2 and Fig. S4). This transient increase in H3K36me3 was also manifested in HEK293T cells upon treatment with other agents that induce DNA DSBs, including  $\gamma$  rays and etoposide (Fig. S3). In addition, the temporal response in H3K36me3 parallels that of  $\gamma$ -H2AX (Fig. 1 and Figs. S2&S3), an indicator of DNA DSB levels (24). Moreover, our ChIP-PCR analysis results showed elevated levels of H3K36me3 at a locus proximal to the I-SceI-generated DNA DSB site for chromatin samples isolated at 4 hr following I-SceI transfection (Fig. 4). At first glance, these findings appear to be incongruent with previous ChIP analysis results revealing the lack of increase in H3K36me3 following DNA DSB induction (7,27). However, the previous ChIP experiments were conducted for chromatin samples isolated from cells at much longer time interval following I-SceI transfection (18-24 hr), and our time-course study clearly demonstrated the transient nature of the increase in H3K36me3 (Fig. 1 and Fig. S3-S4).

**DNA damage-induced H3K36me3 enhances the chromatin binding of LEDGF and KAT5.**

Others have shown that the SETD2-mediated



H3K36me3 is required for DSB repair pathway choice by promoting HR through the recruitment of LEDGF and CtIP to chromatin (7-9). We further substantiated these previous findings by demonstrating that the CRISPR-Cas9-mediated genetic ablation of SETD2 in HEK293T cells substantially perturbed the chromatin localization of LEDGF and that the interaction between histone H3 and LEDGF requires an intact PWWP domain of the latter protein (Fig. 3).

In human cells, H4K16 acetylation is mainly catalyzed by hMOF and KAT5 (28,29). In *MOF*-depleted cells, NHEJ- and HR-mediated repair of DNA DSBs was inhibited (15). KAT5 participates in DNA DSB repair through the NuA4-KAT5 complex, which acetylates histones H2AX and H4 near DSB sites (17,30,31). Furthermore, KAT5 can acetylate lysine residues on non-histone proteins (32). For instance, KAT5 catalyzes the acetylation of ATM, and this acetylation activates ATM and confers heightened cellular resistance toward ionizing radiation (33,34). We found that DNA DSB induction enhances the localization of KAT5, but not hMOF, to chromatin (Fig. 1*G-H*), and this DNA damage-stimulated chromatin localization of KAT5 depends on H3K36me3 and LEDGF (Fig. 1*H&3D*). Thus, we uncovered a novel regulatory mechanism of KAT5 in DNA damage response and repair.

### **H3K36me3-H4K16ac crosstalk in DNA DSB repair.**

Our results revealed a novel histone crosstalk where, upon DNA DSB induction, H3K36me3 stimulates H4K16ac. We found that the DNA damage-induced transient increase in H4K16ac is abolished in human cells depleted of H3K36 trimethyltransferase, SETD2 (Fig. 1). Our notion that H3K36me3 promotes H4K16ac also finds its support from the observation that the increase in H3K36me3 precedes that of H4K16ac following DNA DSB induction (Fig. 1 and 2). H4K16ac is a

very important signal in DNA DSB repair, where it modulates the DSB repair pathway choice (35,36). Introduction of synthetic H4K16ac into nucleosomes was shown to suppress their compaction into 30 nm chromatin fibers (20); thus, H4K16ac elicits an open chromatin environment that is permissive for DNA DSB repair. In addition, elevated acetylation of H4K16 diminishes the binding of 53BP1 to H4K20me2-decorated chromatin, which enhances the binding of BRCA1 to chromatin and HR repair (21,22). Thus, the discovery that H3K36me3 and H4K16ac are mechanistically coupled in HR-mediated repair of DNA DSBs provides important new knowledge about the modulation of DNA repair by histone epigenetic marks. In this respect, it is worth noting that *SETD2* is among the most frequently mutated genes in human cancers (37), and SETD2 is known to function in maintaining genomic integrity (38,39). Our study suggests that SETD2's function in tumor suppression and genomic maintenance may arise from not only its direct role on inducing H3K36me3, but also its indirect impact on promoting H4K16ac.

Taken together, our results support a mechanistic model where DNA DSB induction stimulates the SETD2-dependent H3K36me3 (Fig. 4*D*). Trimethylation of H3K36 promotes the chromatin localization of its reader protein, LEDGF, which binds to KAT5 and facilitates the recruitment of KAT5 to chromatin, thereby elevating H4K16ac. Thus, we revealed a novel crosstalk between H3K36me3 and H4K16ac in the context of DNA DSB repair in human cells, and defined the molecular mechanism for this crosstalk.

### **Experimental procedures**

**Cell culture.** HEK293T, HeLa and U2OS cells were purchased from ATCC (Manassas, VA). U2OS cells harboring a chromosomally integrated

copy of DR-GFP reporter were kindly provided by Prof. Jeremy M. Stark (40). Cells were cultured in Dulbecco's modified Eagle's medium (ATCC) supplemented with 10% fetal bovine serum (FBS, Invitrogen) and 100 unit/mL penicillin/streptomycin. All cells were cultured at 37°C in a humidified incubator with 5% CO<sub>2</sub>.

#### *CRISPR/Cas9-mediated genome editing in HEK293T cells*

CRISPR/Cas9-mediated genome editing was performed as previously described (41,42). An online sgRNA design tool (<http://www.broadinstitute.org/rnai/public/analysis-tools/sgRNA-design>) was employed for designing the single guide RNA (sgRNA). The guide sequences used in this study were (underline indicates the PAM motif):

Human *SETD2* gene:  
AAATATAAATGGATCTCCTGGGG;

Human *MRG15* gene:  
ACCTTTGCTTCATAAAGAAGAGG;

Human *LEDGF* gene:  
TACAAATCACTTACTCGAGCTTGG;

Human *KAT5* gene:  
CAGTGGCAGCCCAGCCAGGACCGG.

Oligodeoxyribonucleotides corresponding to target sequences were obtained from IDT and inserted into the hSpCas9 plasmid pX330 (Addgene, Cambridge, MA, USA). The constructed plasmids were then transfected into HEK293T cells using Lipofectamine 2000 (Invitrogen, Carlsbad, CA, USA) and individual cells were cultured for further analysis. The successful knockout of the corresponding genes was confirmed by genomic DNA sequencing and/or Western blot analyses.

**Histone extraction, chromatin fractionation and Western blot.** Core histones were extracted from cultured human cells following previously published procedures (43). Briefly, cell pellets were washed with a 0.5-mL lysis buffer containing

0.25 M sucrose, 10 mM MgCl<sub>2</sub>, 0.5 mM PMSF, 50 mM Tris (pH 7.4) and 0.5% Triton X-100. The pellets were then resuspended in 0.5 mL of the same buffer and kept at 4°C overnight. The histones were extracted from the cell lysis mixture with 0.4 M sulfuric acid by incubating at 4°C for at least 4 hrs with continuous vortexing. Histones were then precipitated with cold acetone and redissolved in water. For detection of histone modifications, different cell lines were treated with or without NCS (100 ng/mL), etoposide (50 µM) or γ rays (5 Gy), and the cells were harvested at different time points for histone extraction. The NCS-induced temporal alterations in H3K36me3 and H4K16ac in HEK293T cells and the isogenic cells depleted of *SETD2*, *KAT5*, *LEDGF*, or *MRG15* were conducted in at least 3 biological replicates, each of which was performed on a separate day.

Chromatin fractionation was performed following the protocol described by Aygun et al. (44). Briefly, the cells were lysed using a cytoplasmic lysis buffer (10 mM Tris-HCl, pH 8.0, 0.34 M sucrose, 3 mM CaCl<sub>2</sub>, 2 mM MgCl<sub>2</sub>, 0.1 mM EDTA, 1 mM DTT, 0.5% NP-40, protease inhibitor cocktail) for 30 min on ice, and the intact nuclei were subsequently pelleted by centrifugation at 5000 rpm for 2 min. Nuclei were lysed with nuclear lysis buffer (20 mM HEPES, pH 7.9, 1.5 mM MgCl<sub>2</sub>, 1 mM EDTA, 150 mM KCl, 0.1% NP-40, 1 mM DTT, 10% glycerol, protease inhibitor cocktail) by homogenization. After centrifugation at 14000 rpm for 30 min, the chromatin-enriched pellet fraction was incubated in a chromatin isolation buffer (20 mM HEPES, pH 7.9, 1.5 mM MgCl<sub>2</sub>, 150 mM KCl, 10% glycerol, protease inhibitor cocktail and 0.15 unit/µL benzonase (Sigma)) on ice for 2 hrs. Debris was then removed by centrifugation at 5000 rpm for 2 min and the supernatant collected as the chromatin fraction. Protein concentrations in the soluble and

chromatin fractions were determined by the Bradford assay (Bio-Rad). For detection of KAT5, plasmid encoding C-terminally Flag-tagged KAT5 (kindly provided by Dr. Yingli Sun) was transfected into different cell lines prior to chromatin fractionation and Western blot analysis.

For Western blot analysis, protein samples were separated by SDS-PAGE and transferred to a nitrocellulose membrane (Bio-Rad). The membrane was then incubated in a solution containing the appropriate primary antibodies and 5% BSA for 2 hrs. After washing, the membrane was incubated in a 5% blotting grade blocker (Bio-Rad) containing the suitable secondary antibodies for 2 hrs. The immunoblots were detected using ECL Western blotting detection reagent (Amersham). Primary antibodies used in this study included  $\gamma$ -H2AX (Cell Signaling Technology, 9718S; 1:3000), H3K36me3 (Abcam, ab9050; 1:5000), H3 (Cell Signaling Technology, 9715S; 1:10000), H4K16ac (Millipore, 07-329; 1:10000), H4 (Cell Signaling Technology, 13919S; 1:5000), actin (Cell Signaling Technology, 4967S; 1:5000), MRG15 (Cell Signaling Technology, 14098S; 1:3000), LEDGF (Abcam, ab177159; 1:3000), hMOF (Abcam, ab72056; 1:5000), anti-Flag (Cell Signaling Technology, 2368S; 1:8000), and anti-HA (Sigma, H6908; 1:5000).

#### ***Pull-down and immunoprecipitation assay***

For pull-down assay, HEK293T cells were transfected with plasmids encoding KAT5-HA and LEDGF-Flag. Cells were collected and lysed in CelLytic M Cell Lysis Reagent (Sigma) with 1 $\times$  protease inhibitor cocktail (Sigma) for 30 min on ice. After centrifugation, the lysate (supernatant) was incubated with pre-equilibrated Anti-FLAG M2 Affinity Gel (Sigma) or Anti-HA Magnetic Beads (Thermo Fisher Scientific) at 4°C for 4 hrs. Beads were washed with 20 mM Tris (pH 8.0), 100 mM KCl and 0.1% IGEPAL CA-630 (Sigma) for 5 times and boiled in SDS-PAGE loading dye for

SDS-PAGE and Western blot analysis, following the above-described procedures. For immunoprecipitation, HEK293T cells were transfected with plasmids encoding KAT5-HA. The cells were then collected and lysed in CelLytic M Cell Lysis Reagent (Sigma) with 1 $\times$  protease inhibitor cocktail (Sigma) for 30 min on ice. After centrifugation, the lysate (supernatant) was incubated with or without LEDGF antibody at 4°C for 1 hr. The pre-equilibrated Protein A/G Plus Beads (Thermo Fisher Scientific) were subsequently added and incubated at 4°C for 4 hrs. Beads were washed with 20 mM Tris (pH 8.0), 100 mM KCl and 0.1% IGEPAL CA-630 (Sigma) for 5 times and boiled in SDS-PAGE loading dye for SDS-PAGE and Western blot analyses, following the aforementioned procedures.

#### ***Chromatin immunoprecipitation (ChIP) and real-time PCR***

ChIP experiments were conducted as previously described (45). Approximately 2 $\times$ 10<sup>6</sup> cells were used for chromatin isolation. Generally, washed cells were resuspended in douncing buffer (10 mM Tris-HCl, pH 7.5, 4 mM MgCl<sub>2</sub>, 1 mM CaCl<sub>2</sub>, 1 $\times$  protease inhibitor cocktail). After homogenization, micrococcal nuclease (Worthington Biochemicals) was used to fragment the chromatin, and the reaction was terminated by using 0.5 M EDTA. A hypotonic buffer (0.2 mM EDTA, pH 8.0, 0.1 mM benzamidine, 0.1 mM phenylmethylsulfonyl fluoride, 1.5 mM dithiothreitol, 1 $\times$  protease inhibitor cocktail) was then added to the mixture and incubated on ice for 1 hr. ChIP assays were performed with 1  $\mu$ g of anti-H3K36me3 or anti-H4K16ac antibody. Immunoprecipitated chromatin was eluted with a buffer containing 100 mM NaHCO<sub>3</sub> and 1% SDS at 68°C for 2 hrs. DNA was purified using QIAquick PCR Purification Kit (Qiagen) and used for real-time PCR analysis. Real-time PCR was performed using iQ SYBR Green Supermix (Bio-



rad) on the CFX96 Real-Time PCR detection system (Bio-rad). Primers used in real-time PCR were (F1 and F2 refer to DNA fragments that are approximately 500 and 2500 bp away from the I-SceI-induced DSB site, respectively):

ChIP-F1-F:

TCTTCTTCAAGGACGACGGCAACT;

ChIP-F1-R:

TTGTAGTTGTACTCCAGCTTGTGC;

ChIP-F2-F: CCGCGACGTCTGTCGAGAAG;

ChIP-F2-R: GCCGATGCAAAGTGCCGATA.

The siRNA target sequences for SETD2 and LEDGF were 5'-

GAAACCGUCUCCAGUCUGU-3' and 5'-

GCAAUGAGGAUGUGACUAA-3', respectively.

**Acknowledgements.** The authors would like to thank Profs. Jeremy M. Stark and Yingli Sun for providing cell lines and plasmids. This work was supported by the National Institutes of Health (R21 ES025392).

### Conflict of interest

The authors declare that they have no conflicts of interest with the contents of this article.

### Author contributions

L. L. and Y. W. conceived the project, designed the experiments, analyzed the data, and wrote the manuscript. L. L. conducted all the experiments.

### References

1. Zhou, V. W., Goren, A., and Bernstein, B. E. (2011) Charting histone modifications and the functional organization of mammalian genomes. *Nat. Rev. Genet.* **12**, 7-18.
2. Suganuma, T., and Workman, J. L. (2011) Signals and combinatorial functions of histone modifications. *Annu. Rev. Biochem.* **80**, 473-499.
3. Smeenk, G., and van Attikum, H. (2013) The chromatin response to DNA breaks: leaving a mark on genome integrity. *Annu. Rev. Biochem.* **82**, 55-80.
4. Varier, R. A., and Timmers, H. T. (2011) Histone lysine methylation and demethylation pathways in cancer. *Biochim. Biophys. Acta.* **1815**, 75-89.
5. Wagner, E. J., and Carpenter, P. B. (2012) Understanding the language of Lys36 methylation at histone H3. *Nat. Rev. Mol. Cell Biol.* **13**, 115-126.
6. Li, F., Mao, G., Tong, D., Huang, J., Gu, L., Yang, W., and Li, G. M. (2013) The histone mark H3K36me3 regulates human DNA mismatch repair through its interaction with MutS $\alpha$ . *Cell.* **153**, 590-600.
7. Pfister, S. X., Ahrabi, S., Zalmas, L. P., Sarkar, S., Aymard, F., Bachrati, C. Z., Helleday, T., Legube, G., La Thangue, N. B., Porter, A. C., and Humphrey, T. C. (2014) SETD2-dependent histone H3K36 trimethylation is required for homologous recombination repair and genome stability. *Cell Rep.* **7**, 2006-2018.
8. Carvalho, S., Vitor, A. C., Sridhara, S. C., Martins, F. B., Raposo, A. C., Desterro, J. M., Ferreira, J., and de Almeida, S. F. (2014) SETD2 is required for DNA double-strand break repair and activation of the p53-mediated checkpoint. *Elife.* **3**, e02482.
9. Aymard, F., Bugler, B., Schmidt, C. K., Guillou, E., Caron, P., Briois, S., Iacovoni, J. S., Daburon, V., Miller, K. M., Jackson, S. P., and Legube, G. (2014) Transcriptionally active chromatin recruits homologous recombination at DNA double-strand breaks. *Nat. Struct. Mol. Biol.* **21**, 366-374.

10. Fnu, S., Williamson, E. A., De Haro, L. P., Brenneman, M., Wray, J., Shaheen, M., Radhakrishnan, K., Lee, S. H., Nickoloff, J. A., and Hromas, R. (2011) Methylation of histone H3 lysine 36 enhances DNA repair by nonhomologous end-joining. *Proc. Natl. Acad. Sci. USA*. **108**, 540-545.
11. Hayakawa, T., Zhang, F., Hayakawa, N., Ohtani, Y., Shinmyozu, K., Nakayama, J., and Andreassen, P. R. (2010) MRG15 binds directly to PALB2 and stimulates homology-directed repair of chromosomal breaks. *J. Cell Sci.* **123**, 1124-1130.
12. Sy, S. M., Huen, M. S., and Chen, J. (2009) MRG15 is a novel PALB2-interacting factor involved in homologous recombination. *J. Biol. Chem.* **284**, 21127-21131.
13. Dugaard, M., Baude, A., Fugger, K., Povlsen, L. K., Beck, H., Sorensen, C. S., Petersen, N. H., Sorensen, P. H., Lukas, C., Bartek, J., Lukas, J., Rohde, M., and Jaattela, M. (2012) LEDGF (p75) promotes DNA-end resection and homologous recombination. *Nat. Struct. Mol. Biol.* **19**, 803-810.
14. Zhang, P., Du, J., Sun, B., Dong, X., Xu, G., Zhou, J., Huang, Q., Liu, Q., Hao, Q., and Ding, J. (2006) Structure of human MRG15 chromo domain and its binding to Lys36-methylated histone H3. *Nucleic Acids Res.* **34**, 6621-6628.
15. Sharma, G. G., So, S., Gupta, A., Kumar, R., Cayrou, C., Avvakumov, N., Bhadra, U., Pandita, R. K., Porteus, M. H., Chen, D. J., Cote, J., and Pandita, T. K. (2010) MOF and histone H4 acetylation at lysine 16 are critical for DNA damage response and double-strand break repair. *Mol. Cell Biol.* **30**, 3582-3595.
16. Krishnan, V., Chow, M. Z., Wang, Z., Zhang, L., Liu, B., Liu, X., and Zhou, Z. (2011) Histone H4 lysine 16 hypoacetylation is associated with defective DNA repair and premature senescence in Zmpste24-deficient mice. *Proc. Natl. Acad. Sci. USA*. **108**, 12325-12330.
17. Wu, J., Chen, Y., Lu, L. Y., Wu, Y., Paulsen, M. T., Ljungman, M., Ferguson, D. O., and Yu, X. (2011) Chfr and RNF8 synergistically regulate ATM activation. *Nat. Struct. Mol. Biol.* **18**, 761-768.
18. Renaud, E., Barascu, A., and Rosselli, F. (2016) Impaired TIP60-mediated H4K16 acetylation accounts for the aberrant chromatin accumulation of 53BP1 and RAP80 in Fanconi anemia pathway-deficient cells. *Nucleic Acids Res.* **44**, 648-656.
19. Sun, Y., Jiang, X., Xu, Y., Ayrapetov, M. K., Moreau, L. A., Whetstone, J. R., and Price, B. D. (2009) Histone H3 methylation links DNA damage detection to activation of the tumour suppressor Tip60. *Nat. Cell Biol.* **11**, 1376-1382.
20. Shogren-Knaak, M., Ishii, H., Sun, J. M., Pazin, M. J., Davie, J. R., and Peterson, C. L. (2006) Histone H4-K16 acetylation controls chromatin structure and protein interactions. *Science*. **311**, 844-847.
21. Hsiao, K. Y., and Mizzen, C. A. (2013) Histone H4 deacetylation facilitates 53BP1 DNA damage signaling and double-strand break repair. *J. Mol. Cell Biol.* **5**, 157-165.
22. Tang, J., Cho, N. W., Cui, G., Manion, E. M., Shanbhag, N. M., Botuyan, M. V., Mer, G., and Greenberg, R. A. (2013) Acetylation limits 53BP1 association with damaged chromatin to promote homologous recombination. *Nat. Struct. Mol. Biol.* **20**, 317-325.
23. Xu, Y., Gan, E. S., Zhou, J., Wee, W. Y., Zhang, X., and Ito, T. (2014) Arabidopsis MRG domain proteins bridge two histone modifications to elevate expression of flowering genes. *Nucleic Acids Res.* **42**, 10960-10974.
24. Iacovoni, J. S., Caron, P., Lassadi, I., Nicolas, E., Massip, L., Trouche, D., and Legube, G. (2010) High-resolution profiling of gammaH2AX around DNA double strand breaks in the mammalian genome. *EMBO J.* **29**, 1446-1457.

25. Eidahl, J. O., Crowe, B. L., North, J. A., McKee, C. J., Shkriabai, N., Feng, L., Plumb, M., Graham, R. L., Gorelick, R. J., Hess, S., Poirier, M. G., Foster, M. P., and Kvaratskhelia, M. (2013) Structural basis for high-affinity binding of LEDGF PWWP to mononucleosomes. *Nucleic Acids Res.* **41**, 3924-3936.
26. Hu, Y., Scully, R., Sobhian, B., Xie, A., Shestakova, E., and Livingston, D. M. (2011) RAP80-directed tuning of BRCA1 homologous recombination function at ionizing radiation-induced nuclear foci. *Genes Dev.* **25**, 685-700.
27. Pei, H., Zhang, L., Luo, K., Qin, Y., Chesi, M., Fei, F., Bergsagel, P. L., Wang, L., You, Z., and Lou, Z. (2011) MMSET regulates histone H4K20 methylation and 53BP1 accumulation at DNA damage sites. *Nature.* **470**, 124-128.
28. Akhtar, A., and Becker, P. B. (2000) Activation of transcription through histone H4 acetylation by MOF, an acetyltransferase essential for dosage compensation in *Drosophila*. *Mol. Cell.* **5**, 367-375.
29. Ikura, T., Ogryzko, V. V., Grigoriev, M., Groisman, R., Wang, J., Horikoshi, M., Scully, R., Qin, J., and Nakatani, Y. (2000) Involvement of the TIP60 histone acetylase complex in DNA repair and apoptosis. *Cell* **102**, 463-473.
30. Murr, R., Loizou, J. I., Yang, Y. G., Cuenin, C., Li, H., Wang, Z. Q., and Herceg, Z. (2006) Histone acetylation by Trapp-Tip60 modulates loading of repair proteins and repair of DNA double-strand breaks. *Nat. Cell Biol.* **8**, 91-99.
31. Jha, S., Shibata, E., and Dutta, A. (2008) Human Rvb1/Tip49 is required for the histone acetyltransferase activity of Tip60/NuA4 and for the downregulation of phosphorylation on H2AX after DNA damage. *Mol. Cell Biol.* **28**, 2690-2700.
32. Carrozza, M. J., Utley, R. T., Workman, J. L., and Cote, J. (2003) The diverse functions of histone acetyltransferase complexes. *Trends Genet.* **19**, 321-329.
33. Sun, Y., Jiang, X., Chen, S., Fernandes, N., and Price, B. D. (2005) A role for the Tip60 histone acetyltransferase in the acetylation and activation of ATM. *Proc. Natl. Acad. Sci. USA.* **102**, 13182-13187.
34. Sun, Y., Xu, Y., Roy, K., and Price, B. D. (2007) DNA damage-induced acetylation of lysine 3016 of ATM activates ATM kinase activity. *Mol. Cell Biol.* **27**, 8502-8509.
35. Chapman, J. R., Taylor, M. R., and Boulton, S. J. (2012) Playing the end game: DNA double-strand break repair pathway choice. *Mol. Cell.* **47**, 497-510.
36. Panier, S., and Boulton, S. J. (2014) Double-strand break repair: 53BP1 comes into focus. *Nat. Rev. Mol. Cell Biol.* **15**, 7-18.
37. Lawrence, M. S., Stojanov, P., Mermel, C. H., Robinson, J. T., Garraway, L. A., Golub, T. R., Meyerson, M., Gabriel, S. B., Lander, E. S., and Getz, G. (2014) Discovery and saturation analysis of cancer genes across 21 tumour types. *Nature.* **505**, 495-501.
38. Sato, Y., Yoshizato, T., Shiraishi, Y., Maekawa, S., Okuno, Y., Kamura, T., Shimamura, T., Sato-Otsubo, A., Nagae, G., Suzuki, H., Nagata, Y., Yoshida, K., Kon, A., Suzuki, Y., Chiba, K., Tanaka, H., Niida, A., Fujimoto, A., Tsunoda, T., Morikawa, T., Maeda, D., Kume, H., Sugano, S., Fukayama, M., Aburatani, H., Sanada, M., Miyano, S., Homma, Y., and Ogawa, S. (2013) Integrated molecular analysis of clear-cell renal cell carcinoma. *Nat. Genet.* **45**, 860-867.
39. Zhu, X., He, F., Zeng, H., Ling, S., Chen, A., Wang, Y., Yan, X., Wei, W., Pang, Y., Cheng, H., Hua, C., Zhang, Y., Yang, X., Lu, X., Cao, L., Hao, L., Dong, L., Zou, W., Wu, J., Li, X., Zheng, S., Yan, J., Zhou, J., Zhang, L., Mi, S., Wang, X., Zou, Y., Chen, Y., Geng, Z., Wang, J., Liu, X., Yuan, W., Huang, G., Cheng, T., and

- Wang, Q. F. (2014) Identification of functional cooperative mutations of SETD2 in human acute leukemia. *Nat. Genet.* **46**, 287-293.
40. Gunn, A., and Stark, J. M. (2012) I-SceI-based assays to examine distinct repair outcomes of mammalian chromosomal double strand breaks. *Methods Mol. Biol.* **920**, 379-391.
41. Sakuma, T., Nishikawa, A., Kume, S., Chayama, K., and Yamamoto, T. (2014) Multiplex genome engineering in human cells using all-in-one CRISPR/Cas9 vector system. *Sci. Rep.* **4**, 5400.
42. Wu, J., Li, L., Wang, P., You, C., Williams, N. L., and Wang, Y. (2016) Translesion synthesis of O4-alkylthymidine lesions in human cells. *Nucleic Acids Res.* **44**, 9256-9265.
43. Xiong, L., Ping, L., Yuan, B., and Wang, Y. (2009) Methyl group migration during the fragmentation of singly charged ions of trimethyllysine-containing peptides: precaution of using MS/MS of singly charged ions for interrogating peptide methylation. *J. Am. Soc. Mass Spectrom.* **20**, 1172-1181.
44. Aygun, O., Svejstrup, J., and Liu, Y. (2008) A RECQ5-RNA polymerase II association identified by targeted proteomic analysis of human chromatin. *Proc. Natl. Acad. Sci. USA.* **105**, 8580-8584.
45. Maunakea, A. K., Nagarajan, R. P., Bilenky, M., Ballinger, T. J., D'Souza, C., Fouse, S. D., Johnson, B. E., Hong, C., Nielsen, C., Zhao, Y., Turecki, G., Delaney, A., Varhol, R., Thiessen, N., Shchors, K., Heine, V. M., Rowitch, D. H., Xing, X., Fiore, C., Schillebeeckx, M., Jones, S. J., Haussler, D., Marra, M. A., Hirst, M., Wang, T., and Costello, J. F. (2010) Conserved role of intragenic DNA methylation in regulating alternative promoters. *Nature.* **466**, 253-257.

**Figure Legends**

**Fig. 1. Exposure to DNA DSB-inducing agents led to elevated levels of H3K36me3 and H4K16ac, and *SETD2*<sup>-/-</sup> cells exhibited a decreased level of H4K16ac.** (A) The levels of H3K36me3 and H4K16ac were decreased in *SETD2*<sup>-/-</sup> cells, where histones H3 and H4 were used as references, respectively. (B) Quantification of Western blot results showed diminished H3K36me3 and H4K16ac levels in *SETD2*<sup>-/-</sup> cells. (C-F) Time-course experiments showed a transient elevation in the levels of  $\gamma$ H2AX, H3K36me3, and H4K16ac in HEK293T (293T) cells after treatment with 100 ng/mL NCS, where histones H4, H3 and H4 were used as references, respectively. The NCS-induced increase in H4K16ac was abolished in *SETD2*<sup>-/-</sup> cells. Quantification results displayed in (D), (E) and (F) represent the mean and S.E.M. of results obtained from three independent biological replicates conducted on three separate days for all experiments except that the time-course experiment for H3K36me3 was conducted in five independent biological replicates performed on five separate days (See Fig. S2 for Western blot images obtained from other biological replicates). (G-H) The chromatin localization of KAT5, but not hMOF, was increased in HEK293T cells after NCS treatment, and this increase in chromatin binding of KAT5 was lost in *SETD2*<sup>-/-</sup> cells. Actin and histone H3 were employed as loading controls for the soluble (SF) and chromatin (CF) fractions, respectively. The relative values below the lanes were calculated from the ratios of band intensities of CF over SF, which were normalized against actin and histone H3, respectively.

**Fig. 2. Temporal responses of H3K36me3 and H4K16ac levels in different cell lines following DNA DSB induction.** (A-C) Time-course experiments revealed the dynamic changes in H3K36me3 and H4K16ac levels following NCS treatment. Shown are the Western blot results (A) and the quantification data for the relative levels of H3K36me3 and H4K16ac (B-C). The relative levels of these two histone modifications were calculated using histones H3 and H4 as references, respectively. The quantification data represent the mean and S.E.M. of results obtained from three independent biological replicates for all experiments with the exception that the time-course experiment for H3K36me3 was conducted in five independent biological replicates; each biological replicate was conducted on a separate day. Western blot images for data obtained from other biological replicates for *LEDGF*<sup>-/-</sup> and *KAT5*<sup>-/-</sup> cells are shown in Fig. S5.

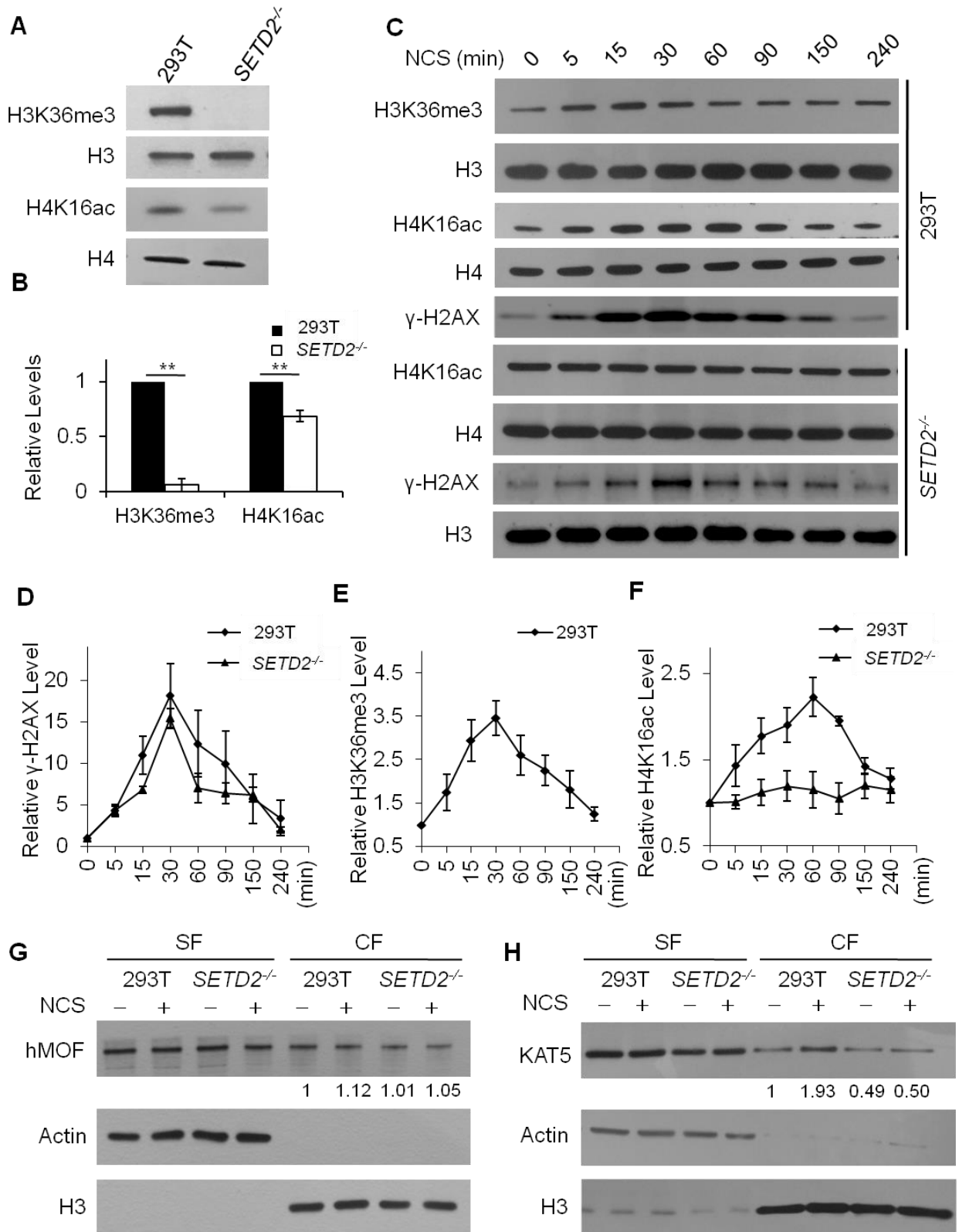
**Fig. 3. LEDGF facilitates the recruitment of KAT5 to chromatin following DNA DSB induction.** (A) Flag-tagged LEDGF, but not LEDGF-Y18AW21A, could pull down histone H3 and H3K36me3. (B) Chromatin localization of LEDGF protein in HEK293T and *SETD2*<sup>-/-</sup> cells. Knockout of *SETD2* confers diminished chromatin localization of LEDGF. (C-D) The chromatin localization of C-terminally Flag-tagged KAT5 (KAT5-Flag), but not hMOF, was increased in HEK293T cells upon NCS treatment, and this increase in chromatin binding of KAT5-Flag was abolished in *LEDGF*<sup>-/-</sup> cells. Actin and histone H3 were employed as loading controls for the soluble (SF) and chromatin (CF) fractions, respectively. The values below the lanes were calculated from the band intensities normalized against histone H3. (E-F) Reciprocal pull-down experiments revealed the interaction between LEDGF and KAT5. KAT5-HA and LEDGF-Flag were co-transfected into cells and pull-down experiments were conducted using anti-HA beads or anti-Flag beads. Results from another biological replicate is shown in Fig. S8F and S8G. (G-H)



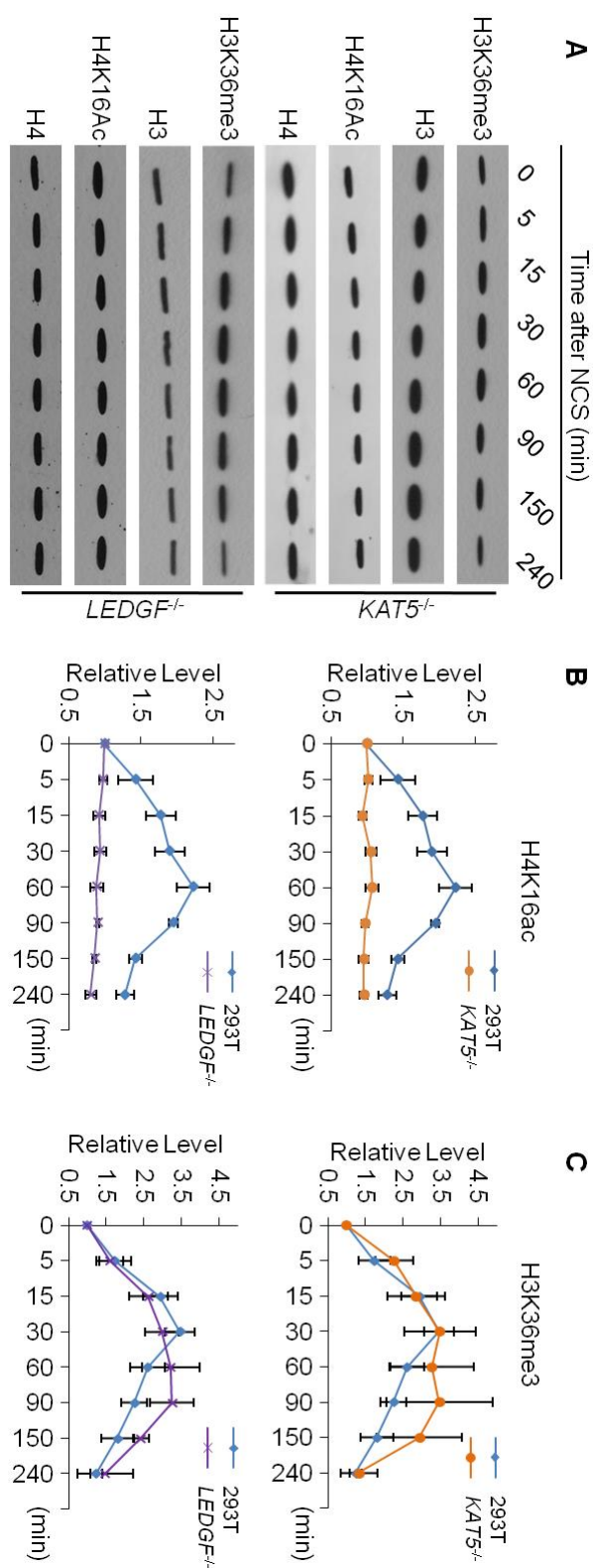
Reciprocal pull-down experiments revealed the interaction between endogenous LEDGF and ectopically expressed HA-KAT5. Results from another biological replicate is shown in Fig. S8H-I. The non-specific band in panel H was labeled with “\*”. LEDGF Ab: LEDGF antibody used for immunoprecipitation.

**Fig. 4. Changes in H3K36me3 and H4K16ac levels around a site-specifically generated DNA DSB site, and the modulations of the levels of these two histone modifications by SETD2 or LEDGF.** (A) A schematic diagram showing the locations of two sets of target fragments used in the ChIP assay. The numbers below indicate the numbers of base pairs (bp) between the target fragments and the I-SceI cleavage site. (B-C) The relative occupancies (enrichment) of H3K36me3 (B) and H4K16ac (C) as revealed by ChIP assay. U2OS cells were transfected with or without siRNA targeting *SETD2* or *LEDGF* gene for 48 hrs. I-SceI plasmid was subsequently transfected into cells and the cells were harvested at 4 hrs following transfection. The cells without I-SceI transfection were used as negative control. For ChIP experiments, the relative enrichment was calculated by comparing the antibody binding results with the amounts of input DNA, and each value was normalized against the negative control without I-SceI transfection. The data represent the mean and S.E.M. of results from three biological replicates. (D) A model showing the H3K36me3-H4K16ac crosstalk in response to DNA DSB induction and the involvement of LEDGF and KAT5 in this crosstalk.

**Fig. 1.**



**Fig. 2.**



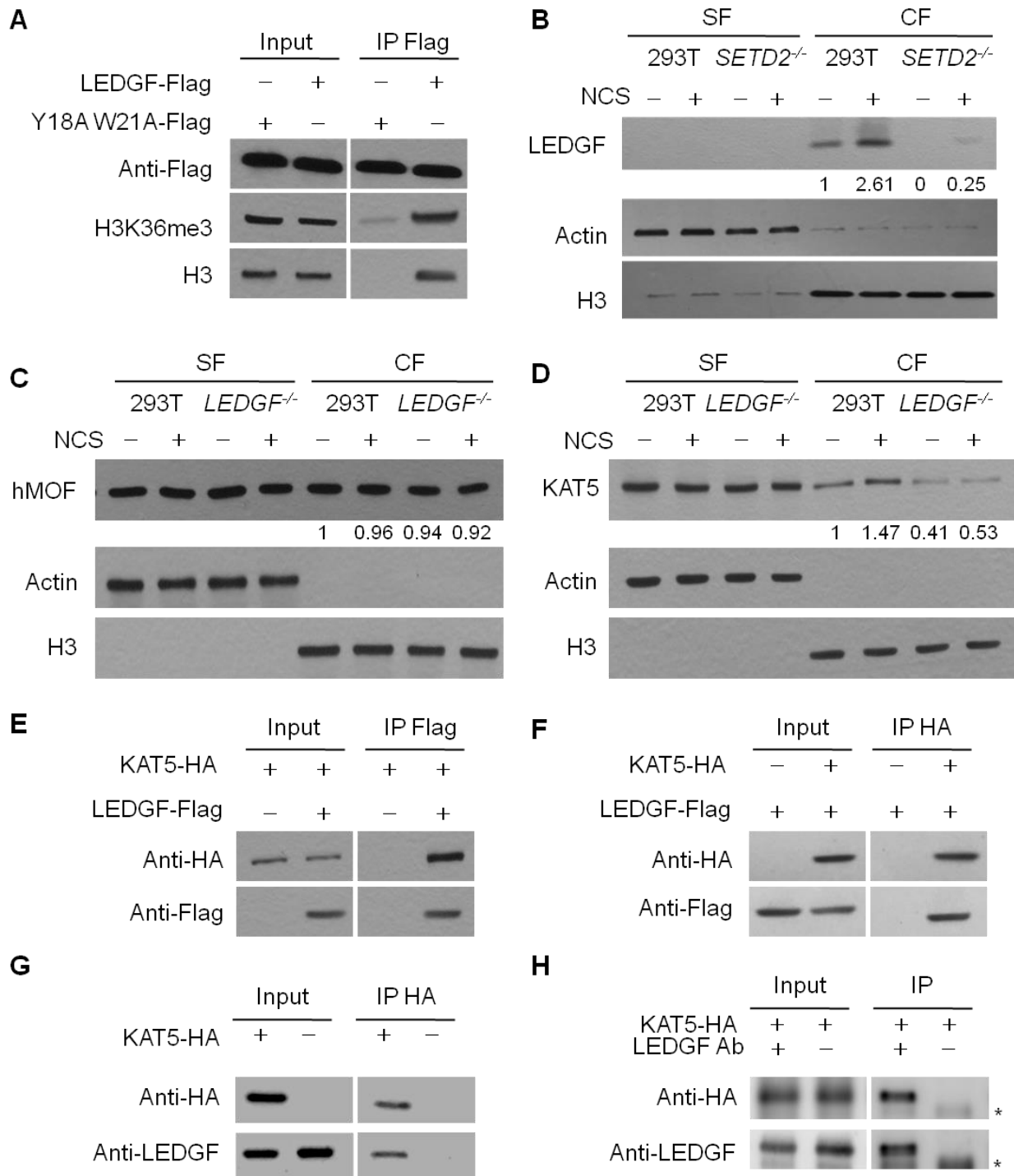
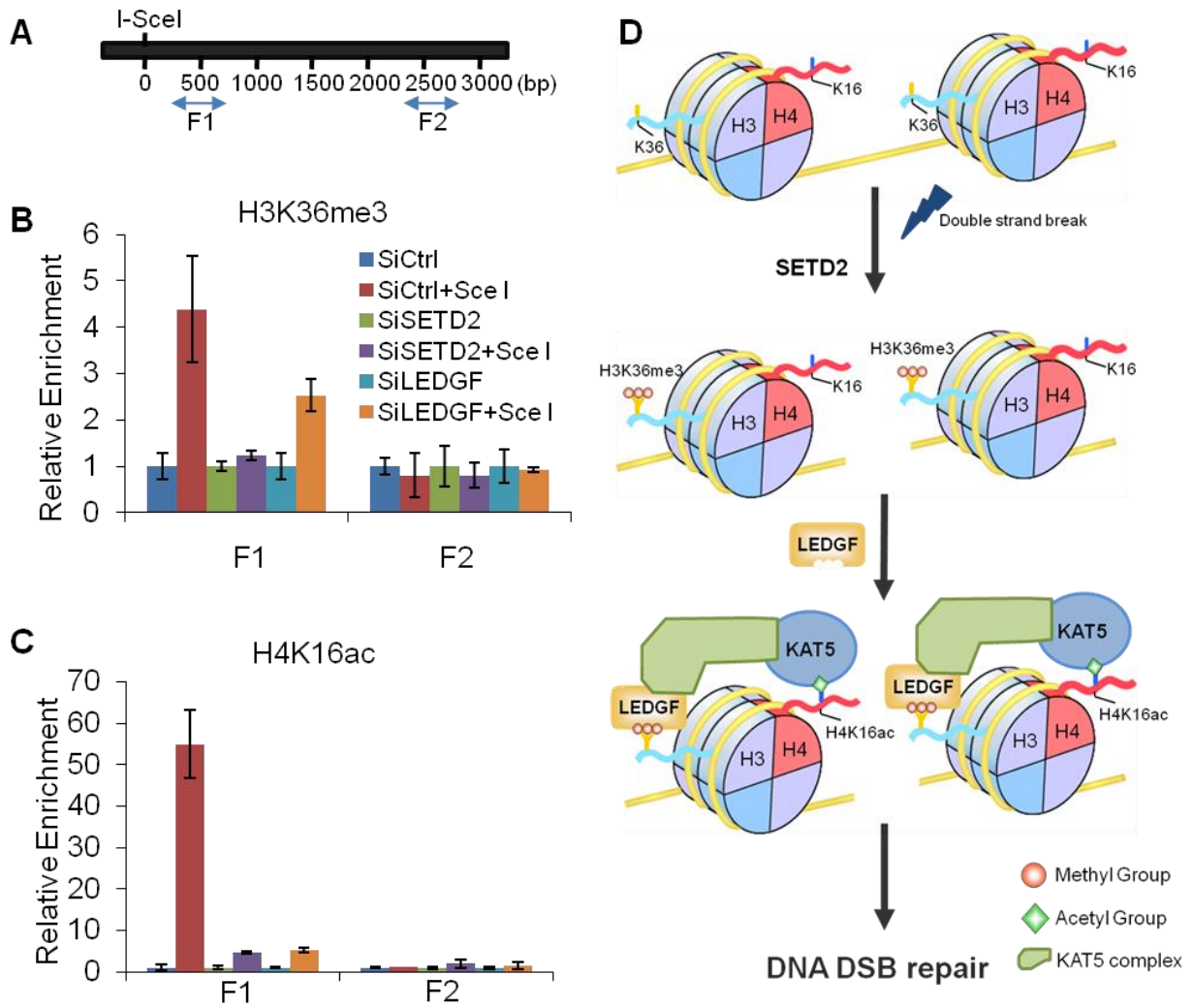
**Fig. 3.**

Fig. 4.





**Crosstalk between the H3K36me3 and H4K16ac histone epigenetic marks in DNA  
double-strand break repair**

Lin Li and Yinsheng Wang

*J. Biol. Chem.* published online May 25, 2017

---

Access the most updated version of this article at doi: [10.1074/jbc.M117.788224](https://doi.org/10.1074/jbc.M117.788224)

Alerts:

- [When this article is cited](#)
- [When a correction for this article is posted](#)

[Click here](#) to choose from all of JBC's e-mail alerts

Supplemental material:

<http://www.jbc.org/content/suppl/2017/05/25/M117.788224.DC1>

This article cites 0 references, 0 of which can be accessed free at

<http://www.jbc.org/content/early/2017/05/25/jbc.M117.788224.full.html#ref-list-1>